Available online at www.sciencedirect.com
SCIENCE DIRECT®
Ultrasonics Sonochemistry 11 (2004) 293–300
Ultrasonics SONOCHEMISTRY
www.elsevier.com/locate/ultsonch

A sonochemical method for the selective synthesis of α-HgS and β-HgS nanoparticles

Hui Wang, Jun-Jie Zhu *

Laboratory of Mesoscopic Materials Science, State Key Laboratory of Coordination Chemistry, Department of Chemistry, Nanjing University, Nanjing 210093, PR China

Received 3 March 2003; received in revised form 30 April 2003; accepted 20 June 2003
Available online 22 September 2003

Abstract

A novel sonochemical method for the selective synthesis of α-HgS (cinnabar) and β-HgS (metacinnabar) nanoparticles in aqueous solutions is reported in this paper. α-HgS and β-HgS nanoparticles have been selectively prepared by choosing sodium thiosulfate and thiourea as the sulfur source respectively. To study the crystalline structure, size, morphology and composition of the products, characterization techniques including X-ray powder diffraction, transmission electron microscopy, selected area electron diffraction, X-ray photoelectron spectroscopy and energy-dispersive X-ray analysis are employed. The optical properties of the nanoparticles are investigated by UV–visible absorption spectroscopic measurements. The direct band gap of the as-prepared α-HgS nanoparticles with an average size of 12 nm is calculated to be 2.8 eV according to the absorption spectrum. In the case of the β-HgS nanoparticles with an average size of 13 nm, a broad absorption peak is observed in the UV–visible absorption spectrum, which can be ascribed to the special surface state of this sample. Probable mechanisms for the sonochemical formation of α-HgS and β-HgS nanoparticles in aqueous solutions are presented. The optimum pH value of the stock solutions and the effect of sonication time on the particle size are also investigated.

Keywords: Sonochemistry; Nanocrystalline; Mercury sulfide; Cinnabar; Metacinnabar

1. Introduction

Currently, the study on physical and chemical effects of ultrasound irradiation is a rapidly growing research area. When liquids are irradiated with high-intensity ultrasound irradiation, acoustic cavitations (the formation, growth, and implosive collapse of the bubbles) provide the primary mechanism for sonochemical effects. During cavitation, bubble collapse produces intense local heating, high pressures and extremely rapid cooling rates [1,2]. These transient, localized hot spots can drive many chemical reactions, such as oxidation, reduction, dissolution, decomposition, and promotion of polymerization [2]. One of the most important recent aspects of sonochemistry has been its applications in the synthesis of nanodimensional materials [3]. Ultrasound irradiation offers a very attractive method for the preparation of novel materials with unusual properties and has shown very rapid growth in its application to materials science due to its unique reaction effects and ability to induce the formation of particles with much smaller sizes [2,3]. The advantages of sonochemcial method include a rapid reaction rate, controllable reaction conditions and the ability to form nanoparticles with uniform shapes, narrow size-distributions and high purity. Up to now, various kinds of nanodimesional materials have been successfully synthesized sonochemically, such as metals [1,4], carbides [5], nitrides [6], oxides [7], chalcogenides [8], and core/shell nanocomposites [9].

Nanoparticles of group II–VI chalcogenides, ME (M = Zn, Cd, Hg; E = S, Se, Te), have attracted an increasing interest during the recent years due to various areas of applications. Mercury sulfide (HgS) is a useful material with wide application in many fields such as ultrasonic transducers, image sensors, electrostatic

* Corresponding author. Tel.: +86-25-3594976; fax: +86-25-3317761.
E-mail address: jjzhu@nju.edu.cn (J.-J. Zhu).

1350-4177/$ - see front matter © 2003 Elsevier B.V. All rights reserved.
doi:10.1016/j.ultsonch.2003.06.002

image materials, and photoelectric conversion devices [10–12]. HgS crystallizes in three different structures among which α-HgS (cinnabar, trigonal type, hexagonal unit cell) and β-HgS (metacinnabar, zincblende type, cubic unit cell) have been most intensively explored. However, up to now, most studies on II–VI chalcogenides have been focused on zinc and cadmium chalcogenides. Reports about the preparation of mercury chalcogenides are relatively scarce due to the toxicity problem of mercuride. Conventional methods for the preparation of mercury chalcogenides include solid-state reaction [13], reaction of metal cation with hydrogen chalcogenides in aqueous solution [14], and molecular precursor methods [15]. However, generally speaking, these methods usually require high reaction temperature (~800 K), and/or involve the use of toxic and highly sensitive precursors (e.g., gaseous hydrogen chalcogenides or organomercury compounds). Over the past few years, much progress has been made in exploring new methods to prepare HgS with nanoscale dimensions with the goals of searching for milder preparation conditions and avoiding the use of toxic reagents or complicated organometallic precursors. Compared with solid state reactions and gas-phase chemical processes, solution-based synthesis is regarded as a more promising approach in terms of much lower cost and potential for high volume production as well as tight dimension control. A variety of solution-based procedures, such as chemical bath deposition [16], room temperature reactions in liquid ammonia [17], ''chemical scissors'' route [18], solvothermal process [19], microwave-assisted heating [20], Langmuir–Blodgett films [21], sol–gel procedure [22], polyol mediated synthesis [23], controlled nucleation/growth in the presence of ligands/surfactant [24], have been developed to prepare nanoscale HgS in forms of solid thin films, colloidal quantum dots, or ultrafine powders.

In this paper, we report a novel sonochemical method for the selective preparation of α-HgS and β-HgS nanoparticles in aqueous solutions under ambient air. It is reported that β-HgS nanoparticles have been prepared previously by Gedanken and co-workers using sonochemical reactions in ethylenediamine [25]. This route is not environmentally friendly due to the toxicity of ethylenediamine. Furthermore, because of the high affinity for complexation of ethylenediamine, there is often a relatively high level of carbon impurity and even incorporation of ethylenediamine in the resulting products [26]. Here, we developed an aqueous sonochemical method to synthesize pure single-phased α-HgS and β-HgS nanoparticles selectively. The products have uniform shape, narrow size-distribution and high purity. It is found to be a convenient, energy efficient and environmentally friendly one-pot method to the selective synthesis of α-HgS and β-HgS nanoparticles.

2. Experimental

All the reagents were of analytical purity, and were used without further purification. Mercury acetate and thiourea were purchased from Guangzhou Chemical Reagent Factory (China). Sodium thiosulfate, 36% acetic acid, triethanolamine (TEA) and ammonia solution were purchased from Nanjing Chemical Reagent Factory (China). Absolute ethanol and acetone were purchased from Shanghai Chemical Reagent Factory (China).

In a typical procedure for the preparation of α-HgS nanoparticles, 3.2 g $Hg(CH_3COO)_2 \cdot 2H_2O$, 5 ml TEA and 3.6 g sodium thiosulfate was introduced into 95 ml distilled water in a 150 ml round-bottom flask. The pH was measured to be 10. Then the mixture was exposed to ultrasound irradiation under ambient air for 60 min. Ultrasound irradiation was accomplished with a high-intensity ultrasonic probe (Xinzhi Co., China; 0.6 cm-diameter; Ti-horn, 20 kHz, 60 W/cm^2) immersed directly in the reaction solution. The sonication was conducted without any cooling, so that a temperature of about 70 °C was reached at the end of the reaction. Nitrogen gas was bubbled through the reaction solution prior to and throughout the sonication to expel the dissolved oxygen/air. Finally a precipitation of red powders was obtained.

To prepare β-HgS nanoparticles, 1.6 g $Hg(CH_3COO)_2 \cdot 2H_2O$ and 0.5 g thiourea were added into distilled water. Acetic acid was added to adjust the pH to 4 and the total volume of stock solution was 100 ml. The mixture was exposed to ultrasound irradiation under ambient air for 30 min. The sonication was conducted with nitrogen gas bubbled through the reaction solution. At the end of the reaction, the temperature of the bulk solution increased to ~70 °C, and a black precipitate was obtained.

The post-reaction treatment procedure is the same for both products. After cooling to room temperature, the precipitates were centrifuged, washed with distilled water, absolute ethanol and acetone in sequence, and dried in air at room temperature. The final products were collected for characterizations. The yields of the as-prepared α-HgS and β-HgS powders were about 70% and 90% respectively. In both cases, the reaction times (60 min for α-HgS, and 30 min for β-HgS) were enough for completing the reactions, because the yields did not increase any more if the reaction time was further prolonged. The products were characterized by X-ray powder diffraction (XRD), transmission electron microscopy (TEM), selected area electron diffraction (SAED), X-ray photoelectron spectroscopy (XPS) and energy-dispersive X-ray analysis (EDAX) and UV–visible absorption spectroscopy.

XRD measurements were performed on a Shimadzu XD-3A X-ray diffractometer with graphite monochromatized CuKα radiation ($\lambda = 0.15418$ nm) and nickel

filter. The acceleration voltage was 35 kV with a 150 mA current flux. Scatter and diffraction slits of 0.5 mm and collection slits of 0.3 mm were used. XRD were taken of the powders attached to a glass slide and data were collected in the 2θ range from 20° to 60°, with a scanning rate of 4°/min and a sample interval of 0.02°. TEM images and SAED pictures were recorded on a JEOL-JEM 200CX transmission electron microscope, using an accelerating voltage of 200 kV. The samples used for TEM observations were prepared by dispersing some products in ethanol followed by ultrasonic vibration for 30 min, then placing a drop of the dispersion onto a copper grid coated with a layer of amorphous carbon. XPS patterns were recorded on ESCALAB MK II X-ray photoelectron spectrometer, using non-monochromatized MgKα X-ray as the excitation source and choosing C1s (284.6 eV) as the reference line. EDAX measurements were performed on the PV9100 instrument. Shimadzu UV-240 photospectrometer was used to record the UV–visible absorption spectra of the as-prepared particles. The sample used for UV–visible absorption measurements were prepared by dispersing some products in ethanol followed by ultrasonic vibration to make a homogeneous suspension with concentrations of approximate 0.2 mg/ml.

3. Results and discussion

To study the crystalline structures of the products, XRD measurements were carried out at room temperature. Fig. 1 shows the XRD patterns of the products. All the reflections in Fig. 1(a) can be indexed to the pure hexagonal (wurtzite structure) phase α-HgS. The peaks are corresponding to (1 0 0), (1 0 1), (0 0 3), (1 0 2) and (1 0 3)..., which matches literature pattern for α-HgS [27] very well. The reflections peaks in Fig. 1(b) are recognized to be a pure cubic (zincblende structure) phase β-HgS. The peaks are corresponding to (1 1 1),

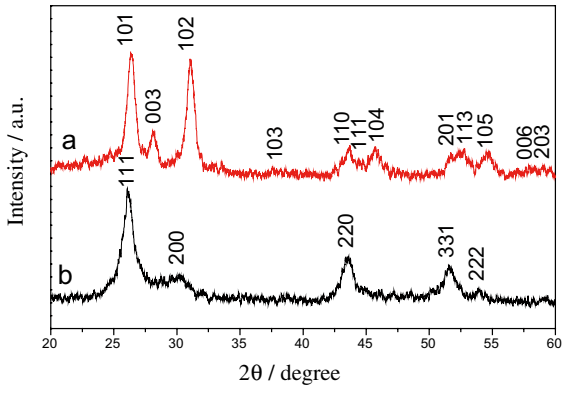

Fig. 1. XRD patterns of the as-prepared: (a) α-HgS; (b) β-HgS nanoparticles.

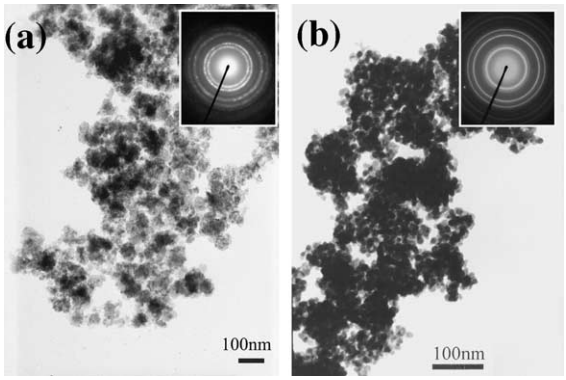

Fig. 2. (a) TEM image of the as-prepared α-HgS nanoparticles, the inset is the corresponding SAED pattern; (b) TEM image of the as-prepared β-HgS nanoparticles, the inset is the corresponding SAED pattern.

(2 0 0), (2 2 0), (3 1 1) and (2 2 2), which are in good agreement with the literature pattern for β-HgS [28]. The broadening of the peaks indicates that the particles are small in size. The average diameters of the as-prepared α-HgS nanoparticles are estimated to be 12 nm and that of β-HgS is calculated to be 13 nm by Debye–Scherrer formula [29] according to the XRD patterns.

The sizes and morphologies of the as-prepared HgS nanoparticles are observed by TEM measurements. In the TEM images (Fig. 2) of the products, it is apparently observed that both α-HgS and β-HgS particles present spherical morphologies. In Fig. 2(a), agglomeration of α-HgS nanoparticles with sizes of 10–13 nm is observed. The as-prepared β-HgS particles are in a better dispersed state. The diameter is observed to be 11–15 nm. The results are in agreement with those estimated by Debye–Scherrer formula from the XRD patterns. The crystallinity and crystallography of the products are proven by SAED results. The inset pictures of Fig. 2 show the SAED patterns of the as-prepared HgS nanoparticles. The SAED measurements indicate that both samples are well crystallized. The diffraction rings are in accord with the corresponding reflection peaks in the XRD patterns.

The products are characterized by XPS and EDAX for the evaluation of their composition and purity. The wide XPS spectrum of the as-prepared β-HgS is shown in Fig. 3(a). The C1s peak lies at 285.1 eV, which should be corrected to 284.6 eV. All the other peaks are corrected accordingly. No peaks of impurities such as oxide or metallic mercury are observed in the spectrum, indicating the high purity of the product. Fig. 3(b) and (c) show the high-resolution XPS spectra of Hg(4f) and S(2p) respectively. The two strong peaks taken for the Hg region at 100.8 and 104.85 eV are assigned to the Hg(4f) binding energy. The peaks measured in the S energy region detected at 162.2 and 163.3 eV are attributed to the S(2p) transitions. Peak areas of Hg(4f)

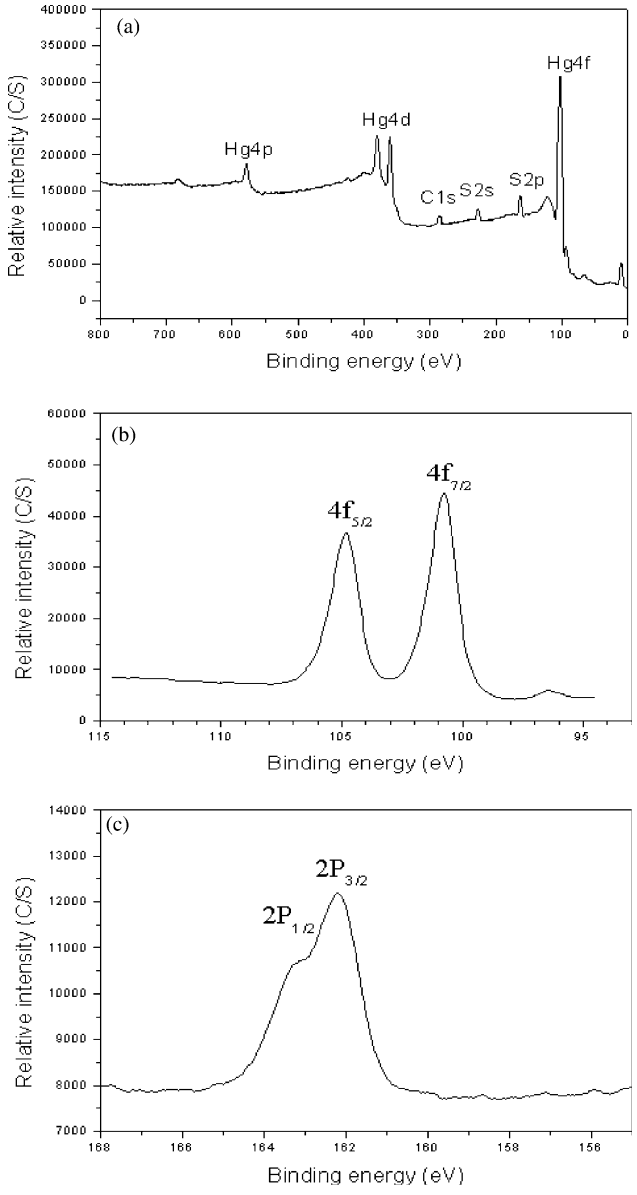

Fig. 3. (a) Wide XPS spectrum of the as-prepared β-HgS nanoparticles; high-resolution XPS spectra taken for the Hg and S region of the as-prepared β-HgS nanoparticles; (b) Hg(4f); (c) S(2p).

and S(2p) are measured and quantification of the peaks gives the ratio of Hg:S to be 56.6:43.4, which indicates that the surface of the sample is rich in Hg. Similar results have been reported previously for HgS nanoparticles [20,25]. XPS primarily monitors concentrations at the surface of the examined samples, which may not be representative of the sample as a whole. The deviation of atomic ratio of Hg:S to the expected 1:1 may be attributed to the excessive Hg^{2+} absorbed on the surface of HgS nanoparticles. According to the XPS spectrum of α-HgS, similar results are obtained. The as-prepared α-HgS nanoparticles also have high purity and the ratio of Hg to S of the product's surface is calculated to be approximately 52.8:47.2. The results of EDAX measurements are consistent with the XPS results.

The study of the optical properties of the materials provides a convenient and effective method for explaining some important features concerning the band structures. The importance of crystal dimensions in the quantum dot size regime is expressed in the variation of the semiconductor energy level structure. We have carried out UV–visible absorption measurements in order to resolve the excitonic or interband transitions of HgS nanoparticles. The UV–visible absorption spectrum of the as-prepared α-HgS nanoparticles homogeneously dispersed in ethanol solution measured at room temperature is shown in Fig. 4(a). The curve ascends sharply from the wavelength at about 600 nm and the optical absorption edge is approximately located at 400 nm. An estimate of the optical band-gap is obtained using the following equation:

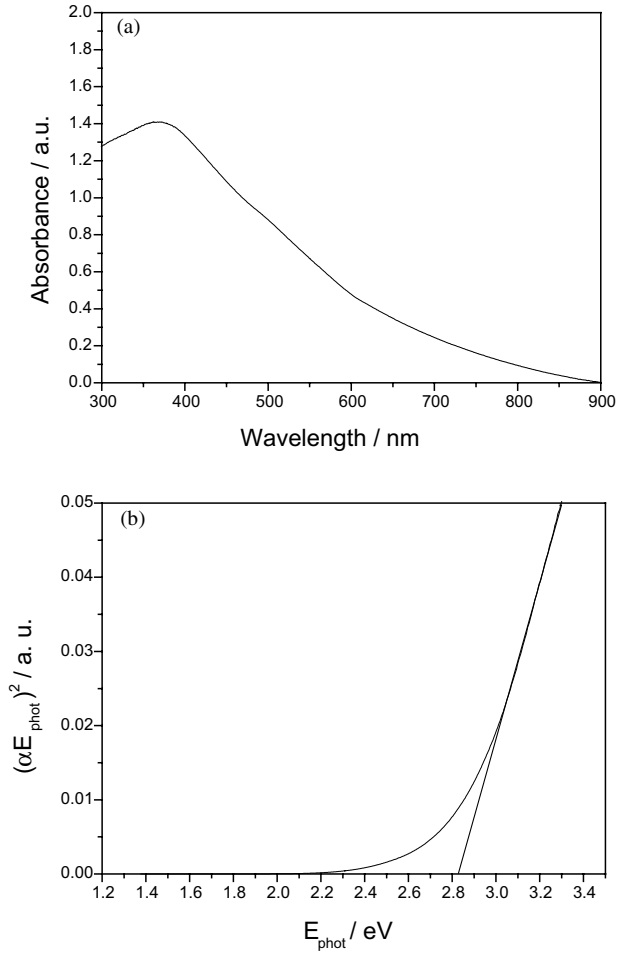

Fig. 4. (a) UV–visible absorbance spectrum of the as-prepared α-HgS nanoparticles; (b) plots of $(\alpha E_{\text{phot}})^2$ vs. E_{phot} for direct transitions, where α is the coefficient and E_{phot} is the photoenergy. The band-gap E_g is obtained by extrapolation to $\alpha = 0$. The data are replotted from Fig. 4(a).

$$\alpha(v) = A(hv/2 - E_g)^{m/2}$$

where A is a constant, α is the absorption coefficient and m equals 1 for a direct transition. The energy intercept of a plot of $(\alpha E_{phot})^2$ versus E_{phot} yields E_g for a direct transition (Fig. 4(b)) [30]. The direct band-gap of the as-prepared α-HgS nanoparticles are calculated to be 2.8 eV according to the UV–visible absorption spectrum, which is larger than the reported value for bulk α-HgS ($E_g = 2.2$ eV) [31]. Light absorption leads to an electron in the conduction band and a positive hole in the valence band. In small particles they are confined to potential wells of small lateral dimension and the energy difference between the position of the conduction band and a free electron, which leads to a quantization of their energy levels. The phenomena arise when the size of the particles becomes comparable to the de Broglie wavelength of a charge carrier. The increase in the band-gap of the as-prepared HgS nanoparticles is the indicative of quantum size effects [32]. Though the common HgS allotrope at room temperature and pressure is α-HgS, β-HgS, the metastable phase is also of great interest because of its (bulk) zero energy bandgap [31]. If the sizes of β-HgS nanoparticles are larger than 10 nm, the optical absorption edge is theoretically located in the near-IR and IR region. However, in the present study, a broad absorption peak centered at about 420 nm is observed in the UV–visible spectrum of the as-prepared β-HgS nanoparticles (Fig. 5). This band can be attributed to the surface state of the β-HgS nanoparticles because the absorption lies below the absorption edge of the particles. The large fraction of surface atoms present in these nanoparticles leads to the large number of dangling bonds and stoichiometric or external defects originating from the surface transition [33]. Similar absorption peaks related to the surface state of nanoparticles have also been observed previously in the case of some other sonochemically synthesized nanoparticles, such as ZnS [9a], ZnSe [8c] and HgS [25].

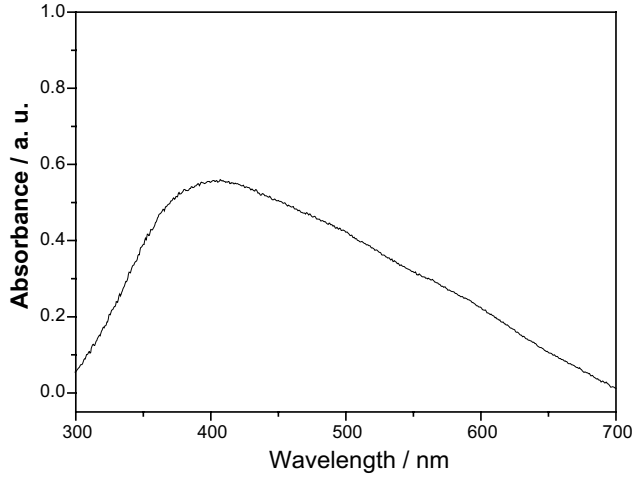

Fig. 5. UV–visible absorption spectrum of the as-prepared β-HgS nanoparticles.

The mechanisms for the formation of α-HgS and β-HgS nanoparticles are probably related to the radical species generated from water molecules by the absorption of the ultrasound energy. It has been known that during an aqueous sonochemical process, the elevated temperatures and pressures inside the collapsing bubbles cause water to vaporize and further pyrolyze into H· and OH· radicals. Prior to and during the sonication, nitrogen gas was bubbled through the reaction solution in order to get rid of the dissolved oxygen, because H· radicals can be quickly scavenged by the oxygen molecules in the solutions to form HOO· radicals [34]. The probable reaction process for the sonochemical formation of α-HgS nanoparticles in aqueous solution can be summarized as follows:

$$H_2O \text{))))))} H^{\cdot} + OH^{\cdot} \quad (1)$$

$$2H^{\cdot} + S_2O_3^{2-} \rightarrow S^{2-} + 2H^{+} + SO_3^{2-} \quad (2)$$

$$Hg^{2+} + S^{2-} \rightarrow HgS \quad (3)$$

$$n\text{HgS} \rightarrow (\text{HgS})_n \quad (4)$$

Reaction (1) represents the formation of primary radicals by the ultrasound-initiated dissociation of water within the collapsing gas bubbles. Reactions (2) and (3) represent the main steps leading to the formation of α-HgS nanoparticles. The H· is a highly reducing radical, and can react with $S_2O_3^{2-}$ ions rapidly via reaction (2) to form S^2 ions [8g]. Then S^{2-} ions combine with Hg^{2+} via reaction (3) to yield HgS nuclei. These freshly formed nuclei in the solution are unstable and have the ability to grow into larger HgS particles and become stable finally. In this process, the as-prepared HgS crystallites exhibit a pure trigonal phase with the hexagonal structure. The reason may be that α-HgS is more stable than β-HgS [35].

The probable mechanism for the formation of β-HgS nanoparticles can be described as below:

$$Hg^{2+} + \text{thiourea} \rightarrow \text{Hg–thiourea complex} \quad (5)$$

$$H_2O \text{))))))} H^{\cdot} + OH^{\cdot} \quad (6)$$

$$2H^{\cdot} + CS(NH_2)_2 \rightarrow H_2S + {}^{\cdot}C(NH_2)_2 \quad (7)$$

$$H_2S + \text{Hg–thiourea} \rightarrow \text{HgS} \quad (8)$$

$$n\text{HgS} \rightarrow (\text{HgS})_n \quad (9)$$

First, the strong complex action between Hg^{2+} and thiourea leads to the formation of Hg–thiourea complex [36]. When exposed to ultrasound irradiation, the excessive thiourea that has not reacted with Hg^{2+} is attacked by the in situ generated H· to form H_2S. Then the

released H_2S reacts with Hg–thiourea complex to produce HgS nanoparticles. Similar ideas have been reported by Gedanken and co-workers when they described the sonochemical reduction of thiourea [8d], selenourea [8c] and thioacetamide [9a] in aqueous solutions. In this case, relatively unstable zincblende phase β-HgS was obtained. Maybe the structure of the Hg–thiourea complex is favorable for the formation of β-HgS nanoparticles with a cubic structure.

To make a comparison, we have carried out control experiments in the absence of the inducement of ultrasound irradiation. In case of α-HgS, when the reaction were carried out with vigorous electromagnetic stir instead of ultrasound irradiation at room temperature (around 20 °C), α-HgS powder could not be obtained even for a sufficient length of time (over 5 h). It shows that ultrasound irradiation provides higher energy than vigorous electromagnetic stir to promote the reactions to form α-HgS nanoparticles. The elevated temperatures and pressures produced during acoustic cavitation may play a major role in the formation of α-HgS nanoparticles. However, β-HgS powder could be obtained after the reaction was carried out with vigorous stir at about 20 °C for over 90 min. The reaction rate became much slower and it took longer period of time for the reaction to be complete. The final precipitate obtained was found to be poorly crystalline according to the SAED pattern (inset in Fig. 6). As observed in the TEM image (Fig. 6), this sample is composed of aggregated particles, and therefore it is difficult to discriminate single particles and measure the individual particle size. These results show that ultrasound irradiation is favorable for the formation of HgS nanoparticles with uniform shape and high crystallinity. It has been known that during the sonochemical process, three different regions [37] are formed: the inner environment (gas phase) of the collapsing bubbles, the interfacial region between the cavitation bubbles and the bulk solution, and the bulk solution, which is at ambient temperature. Among the three regions mentioned above, it appears that the current sonochemical reaction occurs within the interfacial region, yielding nanoparticles, because of the very high quenching rate experienced by the products. If the reactions take place inside the collapsing bubbles, the temperature inside the bubbles depends on the vapor pressure of the solvents. If water is used as the solvent, the maximum bubble core temperature that can be attained is approximately 4000 K [38]. The product is amorphous as a result of the cooling rates ($>10^{10}$ K s^{-1}) which occur during the collapse [2]. On the other hand, if the reactions take place within the interfacial region where the temperature has been measured to be 1900 K [39], one would expect to obtain nanocrystalline products. In the present study, water is used as the solvent and the product is nanocrystalline, which is proven by the results of XRD and SAED measurements. Furthermore, the precursors are ionic in aqueous media, and their vapours are not likely to exist inside the cavitation bubbles due to their low vapour pressure. Though the formation of nanocrystals may also occurs in the bulk solutions, the formation rate is much more rapid in the interfacial region because of the elevated temperature and pressure. Therefore, we propose that the formation of HgS predominantly takes place within the interfacial region.

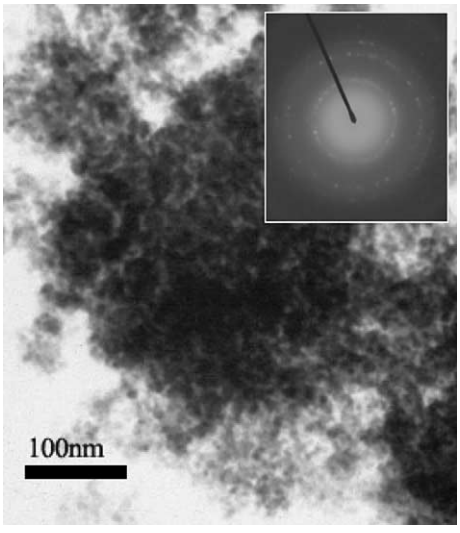

Fig. 6. TEM image and SAED pattern (the inset picture) of β-HgS nanoparticles prepared with vigorous electromagnetic stir for 90 min.

The pH value of the stock solution plays a critical role in the process. To prepare α-HgS nanoparticles, the optimum starting pH should be kept in the range of 9–11. Owing to hydrolysis, aqueous solution of mercury (II) acetate is acidic and if it is mixed with an aqueous solution of sodium thiosulfate, a precipitate is immediately formed as a result of the following reactions [16b]:

$$H^+ + S_2O_3^{2-} \rightarrow S + HSO_3^- \quad (10)$$

$$2S_2O_3^{2-} \rightarrow 2e + S_4O_6^{2-} \quad (11)$$

$$S + 2e \rightarrow S^{2-} \quad (12)$$

$$Hg^{2+} + S^{2-} \rightarrow HgS \quad (13)$$

We found that when this immediate precipitate forms via the above reactions, the product is α-HgS bulk material. In our experiments, TEA was used to adjust the starting pH to 10 to prevent the immediate precipitate. Meanwhile, TEA was a complexing agent which adjusted the concentration of free Hg^{2+} in the solution and was favorable for the formation of particles with small size. We also tried to use ammonia solution to adjust the starting pH to 10. In this case, α-HgS nanoparticles could also be obtained. However, the average particles size increased to ca. 35 nm as observed in the TEM image (Fig. 7).

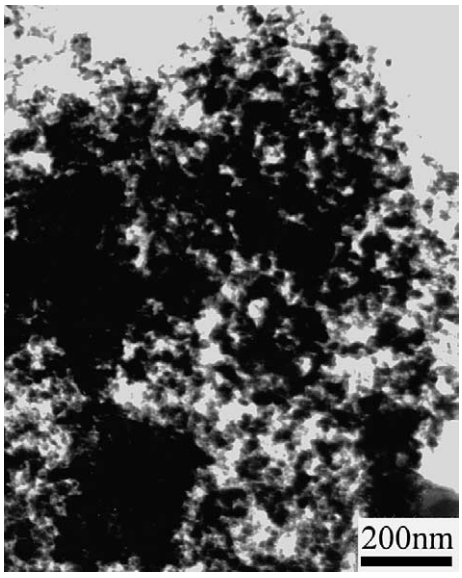

Fig. 7. TEM image of α-HgS nanoparticles prepared sonochemically when ammonia solution was used to adjust the pH to be 10.

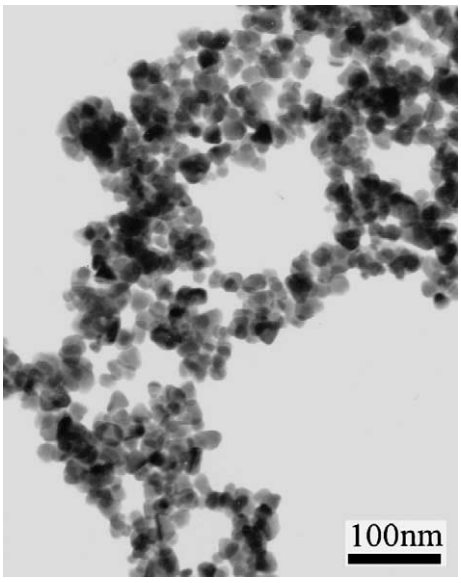

Fig. 8. TEM image of β-HgS nanoparticles obtained after sonication for 1 h.

In the case of β-HgS, the reaction should be carried out in acidic media with pH value in the range of 3–5. In our experiments, we used HAc to adjust the starting pH to 4. In alkaline media, thiourea would react with OH^- to give S^{2-}. As a result, an immediate precipitate would occur, which leads to the formation of β-HgS bulk material. This can be explained as below:

$$2OH^- + CS(NH_2)_2 \rightarrow S^{2-} + CNNH_2 + 2H_2O \quad (14)$$

$$Hg^{2+} + S^{2-} \rightarrow HgS \quad (15)$$

It is also found that the sonication time has influence on the particle size. In the case of β-HgS, we found that after sonication for 30 min, the average diameter of the particles obtained was about 13 nm. If the sonication time was prolonged to 60 minutes, the size of the particles increased to ≈20 nm as can be observed in the TEM image (Fig. 8). We also found that after sonication for over 120 min, the size remained at ≈20 nm. The change of the particle size versus sonication time can be explained by the effect of acoustic cavitation on HgS. The implosive collapse of a cavity on an extended solid surface in a liquid has been recognized to be different from the symmetrical implosion of cavities observed in homogeneous, pure liquids [40]. In the former case, asymmetric implosion results in the formation of high-speed microjets of liquids as well as shock waves that drive the solid particles to high velocities, which leads to interparticle collisions. The collisions between the HgS particles at high velocities result in increased local heating and condensation to form larger particles [41]. The increase in size of the HgS nanoparticles can also involve the crystal growth process. When the HgS nanoparticles formed, smaller particles had a large number of dangling bonds, defect sites, or traps [33a]. After the nucleation of the HgS nuclui, a liquid–solid heterogeneous system forms. In such a system, the presence of ultrasound can enhance the reactions. The effects of interparticle collisions, microjets and shock-waves can drive high-speed jets of liquid to impinge upon the surface which act to create a localized erosion to produce a newly exposed and highly active surface. Meanwhile, the ultrasound improves mass transport, and causes particle fragmentation which substantially increase the surface activity of the solid products which have a large number of dangling bonds, defects or traps on their surface. During the reaction time, the surface states changed. Dangling bonds, defect sites or traps will decrease gradually, and particles will grow. After a period of time under ultrasound irradiation, the surface states become stable gradually. As a result, the size of the β-HgS nanoparticles does not increase any more. The change in surface state of the β-HgS nanoparticles was proven by the disappearance of the absorption peak in the UV–visible absorption spectrum. However, in the case of α-HgS, we did not observe a conspicuous growth process of the as-prepared particles. The probable reason is that the surface state of the α-HgS nanoparticles get stable immediately after the nucleation of α-HgS.

4. Conclusion

In summary, the selective synthesis of α-HgS and β-HgS nanoparticles via a sonochemical route in aqueous solution under ambient air has been established. The products have regular shape, narrow size distribution and high purity. The average sizes of as-prepared

spherical α-HgS and β-HgS nanoparticles are 12 and 13 nm respectively. The mechanisms for the sonochemical formation of α-HgS and β-HgS nanoparticles in aqueous solution are presented. The optimum pH value of the stock solutions and the effect of sonication time on the particle size are also discussed. It is found to be a convenient, mild and efficient route to the synthesis of the HgS nanoparticles with controllable phases.

Acknowledgements

This work is supported by the National Natural Science Foundation of China (No. 50072006 and 90206037) and the Jiangsu Advanced Science and Technology Program (BG 2001039). The authors are also grateful to Mr. Hong Jianmin and Ms. Wang Xiaoshu from Modern Analytic Center at Nanjing University for extending their facilities to us.

References

[1] (a) K.S. Suslick, S.B. Choe, A.A. Cichowlas, M.W. Grinstaff, Nature 353 (1991) 414;
(b) K.S. Suslick, Science 247 (1990) 1439.
[2] K.S. Suslick, Ultrasound: Its Chemical, Physical and Biological Effects, VCH, Weinhein, Germany, 1988.
[3] K.S. Suslick, G.J. Price, Annu. Rev. Mater. Sci. 29 (1999) 295, and the references cited therein.
[4] (a) Y. Koltypin, G. Katabi, R. Prozorov, A. Gedanken, J. Non-Cryst. Solids 201 (1996) 159;
(b) Y. Nagata, Y. Mizukoshi, K. Okitsu, Y. Maeda, Rad. Res. 146 (1996) 333;
(c) K. Okitsu, Y. Mizukoshi, H. Bandow, Y. Maeda, T. Yamamoto, Y. Nagata, Ultrason. Sonochem. 3 (1996) 249.
[5] (a) T. Hyeon, M. Fang, K.S. Suslick, J. Am. Chem. Soc. 118 (1996) 5492;
(b) K.S. Suslick, T. Hyeon, M. Fang, Chem. Mater. 8 (1996) 2172.
[6] Y. Koltypin, X. Cao, R. Prozorov, J. Balogh, D. Kaptas, A. Gedanken, J. Mater. Chem. 7 (1997) 2453.
[7] (a) X. Cao, Y. Koltypin, G. Katabi, I. Felner, A. Gedanken, J. Mater. Res. 12 (1997) 402;
(b) N.A. Dhas, A. Gedanken, J. Phys. Chem. B 101 (1997) 9495;
(c) R.V. Kumar, Y. Diamant, A. Gedanken, Chem. Mater. 12 (2000) 2301;
(d) A. Patra, E. Sominska, S. Ramesh, Y. Koltypin, Z. Zhong, H. Minti, R. Reisfeld, A. Gedanken, J. Phys. Chem. B 103 (1999) 3361.
[8] (a) M.M. Mdleleni, T. Hyeon, K.S. Suslick, J. Am. Chem. Soc. 120 (1998) 6189;
(b) J.Z. Sostaric, R.A. Caruso-Hobson, P. Mulvaney, F. Grieser, J. Chem. Soc. Faraday Trans. 93 (1997) 1791;
(c) J.J. Zhu, Y. Koltypin, A. Gedanken, Chem. Mater. 12 (2000) 73;
(d) P. Jeevanandam, Y. Koltypin, Y. Gofer, Y. Diamant, A. Gedanken, J. Mater. Chem. 10 (2000) 2769;
(e) H. Wang, J.J. Zhu, J.M. Zhu, H.Y. Chen, J. Phys. Chem. B 106 (2002) 3848;
(f) R. Harpenness, O. Palchik, A. Gedanken, V. Palchik, S. Amiel, M.A. Slifkin, A.M. Weiss, Chem. Mater. 14 (2002) 2094;
(g) G. Wang, G. Li, C. Liang, L. Zhang, Chem. Lett. (2001) 344.
[9] (a) N.A. Dhas, A. Zaban, A. Gedanken, Chem. Mater. 11 (1999) 806;
(b) N.A. Dhas, A. Gedanken, Appl. Phys. Lett. 72 (1998) 2514;
(c) M.L. Breen, A.D. Dinsmore, R.H. Pink, S.B. Qadri, B.R. Ratna, Langmuir 17 (2001) 903.
[10] N. Tokyo, Jpn. Kokai Pat. 75130378 (C1.H01L.C01B), 1975.
[11] N. Tokyo, K. Azkio, Jpn. Kokai Pat. 7855478 (C1.C23C15/00), 1978.
[12] N. Tokyo, J. Appl. Phys. 46 (1975) 4857.
[13] T. Ohmiya, Y. Suge, Jpn. J. Appl. Phys. 9 (1970) 840.
[14] I.K. Taimni, Anal. Chim. Acta. 12 (1955) 519.
[15] M.L. Steigerwald, C.R. Sprinkle, J. Am. Chem. Soc. 109 (1987) 7200.
[16] (a) S.S. Kale, C.D. Lokhande, Mater. Chem. Phys. 59 (1999) 242;
(b) M.Z. Najdoski, I.S. Grodanov, S.K. Dey, B.B. Siracevska, J. Mater. Chem. 8 (1998) 2213.
[17] (a) G. Henshaw, I.P. Parkin, G.A. Shaw, J. Chem. Soc. Dalton Trans. 231 (1997);
(b) Y.D. Li, Y. Ding, H.W. Liao, Y.T. Qian, J. Phys. Chem. Solids 60 (1999) 965.
[18] Y. Xie, P. Yan, Y.T. Qian, Chem. Lett. 331 (1999) 655.
[19] J.H. Zeng, J. Yang, Y.T. Qian, Mater. Res. Bull. 36 (2001) 343.
[20] H. Wang, J.R. Zhang, J.J. Zhu, J. Cryst. Growth 233 (2001) 829.
[21] D.J. Elliot, D.N. Furlong, F. Grieser, Colloids Surf. A 155 (1999) 101.
[22] M. Guglielmi, A. Martucci, J. Sol–gel Sci. Tech. 11 (1998) 229.
[23] C. Feldmann, C. Metzmacher, J. Mater. Chem. 11 (2000) 2603.
[24] K.A. Higginson, M. Kuno, J. Bonevich, S.B. Qadri, M. Yousuf, H. Mattoussi, J. Phys. Chem. B 106 (2002) 9982.
[25] J.J. Zhu, S.W. Liu, O. Palchik, Y. Koltypin, A. Gedanken, J. Solid State Chem. 153 (2000) 342.
[26] J. Li, Z. Chen, R.J. Wang, D.M. Prospero, Coord. Chem. Rev. 190–192 (1999) 707.
[27] Joint Committee on Powder Diffraction Standards (JCPDS), File No. 6-256.
[28] Joint Committee on Powder Diffraction Standards (JCPDS), File No. 6-261.
[29] H. Klug, L. Alexander, X-ray Diffraction Procedures, Wiley, New York, 1962, p. 125.
[30] S. Tsunekawa, T. Fukuda, A. Kasuya, J. Appl. Phys. 87 (2000) 1318.
[31] W.L. Roth, in: M. Aven, J.S. Prener (Eds.), Physics and Chemistry of II–VI Compounds, North-Holland, Amsterdam, 1967.
[32] J.P. Yang, F.C. Meldrum, J.H. Fendler, J. Phys. Chem. 99 (1995) 5500.
[33] (a) W. Chen, Z. Wang, Z. Lin, L. Lin, J. Appl. Phys. 82 (1997) 3111;
(b) D. Hayes, O.I. Micic, M.T. Nenadovic, V. Swayambunathan, D. Meisel, J. Phys. Chem. 93 (1989) 4603;
(c) V. Swayambunathan, D. Hayes, K. Schmit, K.H. Schmit, Y.K. Liao, D. Meisel, J. Am. Chem. Soc. 112 (1990) 3831.
[34] E.J. Hart, A. Henglein, J. Phys. Chem. 89 (1985) 4342.
[35] F.A. Cotton, in: G. Wilkinson (Ed.), Advanced Inorganic Chemistry, third ed., JohnWily & Sons Inc., New York, 1972.
[36] Wuhan University and Jilin University et al., 1993. Inorganic Chemistry, third ed. High Education Press, Beijing.
[37] K.S. Suslick, D.A. Hammerton, R.E. Cline, J. Am. Chem. Soc. 108 (1986) 5641.
[38] V. Misik, N. Miyoshi, P. Riesz, J. Phys. Chem. 99 (1995) 3605.
[39] W.B. McNamara, Y.T. Didenko, K.S. Suslick, Nature 401 (1999) 772.
[40] W. Lauterborn, A. Vogel, Ann. Rev. Fluid Mech. 16 (1984) 223.
[41] S. Ramech, Y. Koltypin, A. Gedanken, J. Mater. Res. 12 (1997) 3271.